J Mater Sci (2006) 41:5021–5024
DOI 10.1007/s10853-006-0124-6

LETTER

Nanoscale pseudoelasticity of single-crystal Cu–Al–Ni shape-memory alloy induced by cyclic nanoindentation

H.-S. Zhang · K. Komvopoulos

Received: 17 October 2005 / Accepted: 27 December 2005 / Published online: 13 May 2006

Shape-memory alloys (SMA) have become important structural materials of dynamic microsystems and bioimplants because of their ability to undergo large reversible strains (typically ~8%) by shear dominated, thermoelastic, displacive phase transformations and crystallographic twinning processes. Advances in nanotechnology and microelectromechanical devices have turned the research attention to nanoscale material behavior. Single-crystal Cu–Al–Ni alloy exhibits the largest reversible strain (e.g., 17%) among SMA as well as high thermal and electrical conductivity [1–3]. In addition to the common type of pseudoelasticity associated with phase transformation from the high-temperature austenite (parent) phase to the low-temperature martensite (derivative) phase and vice versa, Cu–Al–Ni demonstrate another type of pseudoelastic behavior involving only martensitic transformations without the formation of austenite.

Previous studies have provided valuable information about phase transformations in single-crystal Cu–Al–Ni alloy and associated stress–strain responses [2, 4]. Four types of martensite phases (α_1', β_1', β_1'', and γ_1') can evolve from the parent austenite (β_1) phase of this SMA under different stress and temperature conditions. For example, β_1' emerges upon excessive deformation of the β_1 phase at an elevated temperature [5, 6] γ_1' can be produced by cooling stress-free austenite [6], and β_1'' and α_1' phases can be formed by stretching the γ_1' phase [4]. Heating may result in transformation back to the austenitic parent phase, hence resulting in full recovery of the original shape.

H.-S. Zhang · K. Komvopoulos (✉)
Department of Mechanical Engineering, University of California, Berkeley, CA 94720, USA
e-mail: kyriakos@me.berkeley.edu

In addition to the bulk behavior of SMA, the nanoscale behavior of films possessing austenitic or martensitic TiNi microstructures at room temperature have been the objective of earlier nanoindentation studies [7–11], and real-time observation of austenite–martensite phase transformation phenomena has been accomplished by in-situ transmission electron microscopy (TEM) [12]. However, fundamental studies of the nanoscale deformation behavior of Cu–Al–Ni (especially pseudoelasticity under cyclic loading) have not been reported to date. Therefore, the objective of this study was to examine the deformation of single-crystal Cu–Al–Ni subjected to tensile loading and nanoindentation and to interpret the underlying nanoscale deformation mechanisms in the light of similarities between macroscopic and nanoscopic behaviors.

Cylindrical samples of single-crystal Cu–Al–Ni were fabricated from a molten pool of 82 wt% Cu, 14 wt% Al, and 4 wt% Ni by using the Czochralski method. The obtained samples of 0.25 inches in diameter were heated at ~870 °C and subsequently cooled rapidly to attain a cubic austenitic microstructure. TEM studies revealed that the room-temperature microstructure consisted of a Cu_3Al-compound (i.e., Fe_3Al-type DO_3 structure) austenite. It is presumed that some random Cu atoms in the lattice structure were replaced by Ni atoms [4]. Differential scanning calorimetry showed that the start and finish austenite (A) and martensite (M) temperatures were $A_s = -36$ °C, $A_f = -31$ °C, $M_s = -38$ °C, and $M_f = -43$ °C, respectively. The cylindrical samples were cut into wires of 0.18 inches in diameter by electrical discharge machining in order to fit in the apparatus for tensile testing and also to plates of 0.02 inches in thickness for use in the nanoindentation experiments. The wire samples did not receive any surface treatment; however, the surfaces of the plate samples were polished sequentially with SiC abrasive

paper of progressively finer grit size and Al_2O_3 abrasive cloth of grit size equal to 30 and 1 μm.

Strain- and temperature-control experiments were performed with a custom-made tension apparatus. A temperature resolution of about ±1 °C was achieved by using an electrical heating stage and a cold nitrogen gas regulator. Nanoindentation experiments were performed with an atomic force microscope (Nanoscope II, Digital Instruments) equipped with a force transducer (Triboscope, Hysitron, Inc.). All the nanoindentations were produced with a Berkovich diamond tip of nominal radius of curvature equal to ~290 nm. The tip radius was determined from a Hertz analysis for the contact depth of an indentation produced on a quartz sample due to a normal load of 50 μN. A triangular loading function with loading and unloading rates both equal to 10 μN/s was used in all the nanoindentation experiments. In the following, stress–strain results from cyclic tensile tests are presented first to establish a reference for comparison with the cyclic nanoindentation results discussed subsequently.

Tensile tests performed by loading austenitic Cu–Al–Ni wires in the [001] direction at room temperature yielded fully reversible strains up to 10% attributable to $\beta_1 \rightarrow \beta_1'$ phase transformation. This type of pseudoelastic behavior resulting from austenite–martensite phase transformation is typical of most SMA [3]. However, a unique deformation behavior was observed at −30 °C, i.e., close to A_f. Figure 1 shows the tensile stress (σ) versus strain (ε) curves of four consecutive loading cycles. In the first cycle, the specimen was deformed up to point A and then unloaded to point B to produce a residual strain of 4.3%. The initial loading up to point A resulted in $\beta_1 \rightarrow \gamma_1'$ phase transformation and, probably, formation of some intermediate β_1' martensite

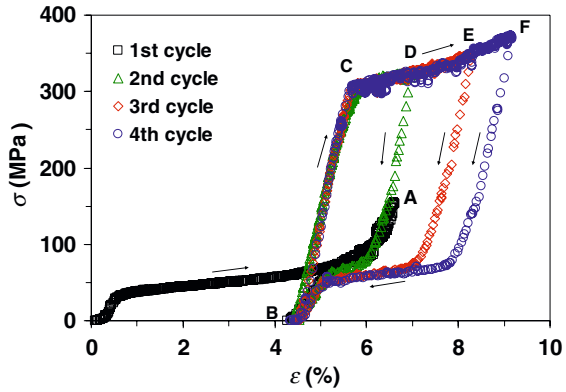

Fig. 1 Stress–strain response of single-crystal Cu–Al–Ni alloy at −30 °C produced from cyclic tensile loading. The first cycle consists of loading up to point A and then unloading to point B. All three consecutive loading cycles begin and end at point B, attaining their corresponding maximum stresses at points D, E, and F. These cycles demonstrate the occurrence of a stable pseudoelastic behavior after the first cycle (training period). The arrows indicate the loading and unloading paths of each stress–strain cycle

phase [13]. The external stress provided the driving force to produce a martensitic microstructure from austenite and to reduce the crystallographic symmetry [8]. However, reverse phase transformation ($\gamma_1' \rightarrow \beta_1$) did not occur upon unloading from A to B as evidenced by the significantly higher slope of the subsequent loading path. It is presumed that the low temperature inhibited the movement of the austenite–martensite interfaces, yielding a microstructure consisting of pure γ_1' martensite (point B) [13]. All three subsequent loading cycles (i.e., BCDB, BCEB, and BCFB) demonstrated a pseudoelastic behavior attributed to fully reversible $\gamma_1' \rightarrow \beta''$ and $\beta_1'' \rightarrow \gamma_1'$ transformations commencing at stress levels above 320 MPa (i.e., points D, E, and F in Fig. 1) and below 100 MPa, respectively. The removal of the external stress caused the microstructure to reverse to that corresponding to point B in order to minimize the free energy. This produced a large hysteresis area, which represents the energy dissipated by phase transformation. A comparison of the loading slopes of the pseudoelastic and first-cycle responses shows that the elastic modulus of the microstructure consisting of the γ_1' phase is significantly higher than that of the original austenitic (β_1) microstructure.

Phase transformation comprises microstructure changes involving energy dissipation [8]. All the martensite phases of Cu–Al–Ni consist of the same six types of stacking planes produced from the cubic β_1 phase but differ in their periodic stacking structures [1, 2]. Stress gradients induced shuffling and rearrangement of the stacking planes leading to phase transformation. Unlike macroscopic tensile tests, nanoindentation produces high stress gradients in the vicinity of the penetrating tip. It was found that fully reversed transformation to the austenite parent phase of Cu–Al–Ni did not occur in the first nanoindentation cycle. However, a pseudoelastic response emerged after a certain number of nanoindentation cycles (training period). Figure 2 shows the contact load L versus tip displacement h response of austenitic Cu–Al–Ni indented in the [001] direction at room temperature for L_{max} = 150 μN. It can be seen that a steady-state pseudoelastic behavior was attained after three consecutive cycles. Further cyclic indentation yielded overlapping load hystereses. The nanoindentation cycles (training period) for attaining a stable pseudoelastic behavior increased with the maximum contact load (e.g., five cycles for L_{max} = 300 μN). It is also shown that during the training period the hysteresis area decreases, while the elastic stiffness (reflected by the slope of the unloading curve at L_{max}) increases as the material approaches a pseudoelastic state. Stable pseudoelastic behavior was obtained for L_{max} in the range of 50–450 μN.

To compare the macroscale and nanoscale deformation behaviors, the nanoindentation force and displacement data were converted to mean stress (σ_m) and representative

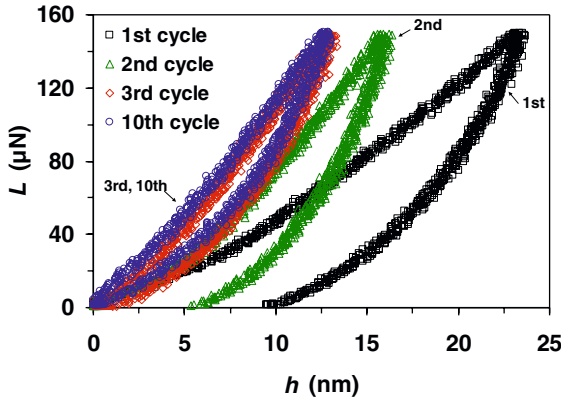

Fig. 2 Nanoindentation curves of single-crystal Cu–Al–Ni alloy at room temperature illustrating a stable pseudoelastic behavior after three nanoindentation cycles (training period) for a maximum load of 150 μN

strain (ε_r), respectively. The mean stress was calculated by dividing the contact load by the corresponding contact area. To determine the contact area as a function of the tip displacement (contact depth), the Berkovich tip was calibrated by performing indentations on a standard fused quartz sample. This procedure led to the determination of the contact area as a polynomial function of the contact depth [14]. The apex of the indenter tip was approximated by a sphere, and the representative strain was obtained by $\varepsilon_r = 0.2\ a/R$, where R is the tip-apex radius of curvature and a is the radius of the contact area corresponding to a certain load (depth) [15]. This assumption is reasonable because the maximum indentation depth in the experiments used to determine the representative strain was <50 nm, which is significantly less than the nominal tip radius.

Figure 3 shows mean stress versus representative strain curves obtained from load versus displacement responses by using the procedure described previously. Data for displacements less than 5 nm are not shown in Fig. 3 because the contact area function could not be determined accurately for such small contact depths. The effect of the high stress gradients in the vicinity of the tip on the transformation of the austenite phase is analogous to lowering the temperature [1]. Therefore, the behavior demonstrated by the first nanoindentation cycle at room temperature can be contrasted with that shown in Fig. 1. As mentioned earlier, continuous tensile deformation of single-crystal Cu–Al–Ni at −30 °C comprised several phase transformations (i.e., $\beta_1 \rightarrow \beta_1' \rightarrow \gamma_1' \rightarrow \beta_1''$). The σ_m vs. ε_r response shown in Fig. 3a can be used in conjunction with Fig. 1 to interpret the plausible phase transformations induced by nanoindentation. For $\varepsilon_r < 0.08$, the response resembles that shown in Fig. 1 for $\varepsilon < 0.01$ and is attributed to the deformation of the β_1 phase. In the range $0.08 < \varepsilon_r < 0.13$, the curve levels off and σ_m changes slightly with increasing deformation. This is also similar to the macroscopic behavior encountered at a critical stress resulting in $\beta_1 \rightarrow \gamma_1'$ transformation (e.g., strain range of 0.01–0.05 in Fig. 1). It is likely that limited $\gamma_1' \rightarrow \beta_1''$ phase transformation also occurred in small regions of high stress gradients adjacent to the contact interface. The unloading curves shown in Fig. 3a reveal differences in both the slope and the residual strain, which may be attributed to variations in the γ_1' and β_1''contents produced by the increase of the strain. Figure 3a shows representative σ_m vs. ε_r curves for a maximum strain of 0.13. Results for $\varepsilon_r > 0.13$ (not shown here for brevity) indicated that the behavior was affected predominantly by plastic deformation, whereas the effect of phase transformation was secondary. As a consequence, a pseudoelastic behavior was not observed for $\varepsilon_r > 0.13$.

The mechanisms affecting the nanoindentation response can be interpreted in terms of the zone-like structure produced under the tip consisting of a plastically deformed zone adjacent to the apex of the tip, a phase transformation zone surrounding the plastic zone, and an outer zone of

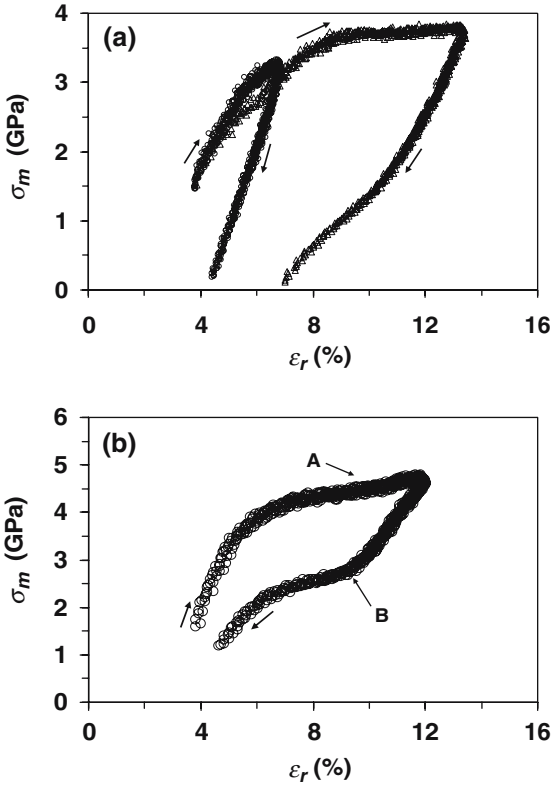

Fig. 3 Stress–strain responses of single-crystal Cu–Al–Ni alloy at room temperature derived from cyclic nanoindentation results: (**a**) first-cycle response for a maximum load of 100 and 450 μN revealing changes in the dominant deformation mechanism(s) and (**b**) stress–strain hysteresis of the stable pseudoelastic behavior obtained after six nanoindentation cycles (training period) for a maximum load of 450 μN. The arrows indicate the loading and unloading paths of each stress–strain cycle

elastically deformed material [9]. It was found that the nanoindentation cycles leading to stable pseudoelasticity increased with the maximum strain (load), presumably due to the effect of plastic strain accumulated in the first cycle. Constrained plasticity did not inhibit pseudoelasticity in subsequent indentation cycles provided plastic deformation was localized and, therefore, its effect on the phase transformation mechanisms was negligible.

Figure 3b shows a stable pseudoelastic response obtained after six nanoindentation cycles for L_{max} = 450 μN. In view of the previous results, it is presumed that the material in the tip vicinity consisted mainly of γ_1' martensite. In view of the significant spatial variations of the stresses under the tip, the loading path shown in Fig. 3b is a result of the superimposed effects of the elastic deformation of the γ_1' phase and the $\gamma_1' \rightarrow \beta_1''$ phase transformation, with the contribution of the phase change effect increasing with the stress. Therefore, it appears that the underlying nanoindentation mechanisms exhibited close similarities with those encountered during loading in the pseudoelastic cycles shown in Fig. 1. However, the increase of the slope at point A indicates a change in the local dominant mechanism from $\gamma_1' \rightarrow \beta_1''$ phase transformation to deformation of the produced β_1'' phase. The reverse phenomenon occurred during unloading to point B. Despite the similar characteristics of the pseudoelastic responses shown in Figs. 1 and 3, significantly higher phase-transformation stresses occurred in the nanoindentation tests. There are several explanations for this difference. First, a higher compressive stress than tensile stress is required to produce the same strain [16]. It is well known that the phase-transformation stress increases with temperature [3]. Hence, a second reason for the higher stresses in the nanoscale pseudoelastic response is that the nanoindentation experiments were performed at room temperature, whereas the tensile tests were carried out at −30 °C. A third possible reason for this discrepancy is the nonuniform distribution of the nanoindentation stresses. Large stress gradients in the tip neighborhood resulted in scale-dependent phase transformations. Hence, the stabilization of the γ_1' phase in the nanoindentation experiments required a higher means stress than that of the tensile tests. Clearly, the stability of the γ_1' phase (attained after the training period) is the precursor to the steady-state pseudoelastic behavior of the Cu–Al–Ni alloy demonstrated in Figs. 1–3.

In conclusion, this study demonstrated that single-crystal Cu–Al–Ni can be trained to exhibit a pseudoelastic behavior by cyclic loading up to a certain maximum stress. In view of the similarities of the stress–strain responses obtained from tensile and nanoindentation tests, it was presumed that the training period led to the stabilization of the γ_1' phase. As a consequence, subsequent cyclic loading involved $\gamma_1' \leftrightarrow \beta_1''$ fully reversible phase transformations. Another important contribution of this work is the insight into the nanoscale pseudoelastic behavior of Cu–Al–Ni and associated phase transformation mechanisms derived from comparisons with the known phase transformations occurring under cyclic tensile loading. From an application perspective, the intriguing martensite phase transformation and stress–strain response of Cu–Al–Ni can be used to design microdevices exhibiting high dynamic agility. For instance, the prospect of alternating between pseudoelastic responses resulting from austenite–martensite and martensite–martensite phase transformation mechanisms through local temperature control so that to perform nanoscale tuning of the damping ratio is a captivating concept worthy of further investigation.

Acknowledgments The authors gratefully acknowledge Dr. A. D. Johnson for helpful discussions and Professor N. Balsara at the University of California at Berkeley for the use of the differential scanning calorimetry equipment.

References

1. Fremont M, Miyazaki S (1996) Shape memory alloys Springer, New York
2. Funakubo, H (1987) Shape memory alloys, translated from the Japanese by J. B. Kennedy. Gordon and Breach Science, New York
3. Duerig TW, Melton KN, Stöckel D, Wayman CM (1990) Engineering aspects of shape memory alloys. Butterworth-Heinemann, London, UK
4. Otsuka K, Shimizu K (1979) Acta Metall 27:585
5. Šittner P, Hashimoto K, Kato M, Tokuda M (2003) Scripta Mater 48:1153
6. Šittner P, Novák V (2000) Int J Plast 16:1243
7. Ni W, Cheng Y-T, Grummon DS (2002) Appl Phys Lett 80:3310
8. Ma X-G, Komvopoulos K (2003) Appl Phys Lett 83:3773
9. Shaw GA, Stone DS, Johnson AD, Ellis AB, Crone WC (2003) Appl Phys Lett 83:257
10. Ma X-G, Komvopoulos K (2004) Appl Phys Lett 84:4274
11. Komvopoulos K, Ma X-G (2005) Appl Phys Lett 87:263108
12. Ma X-G, Komvopoulos K (2005) J Mater Res 20:1808
13. Picornell C, Pons J, Cesari E (2001) Acta Mater 49:4221
14. Thurn J, Cook RF (2002) J Mater Res 17:1143
15. Johnson KL (1985) Contact mechanics. Cambridge University Press, Cambridge, UK
16. Liu Y, Xie Z, van Humbeeck J (1999) Mater Sci Eng A 273–275:673